Joint role exploration in sagittal balance by optimizing feedback gains

Dengpeng Xing and Jianbo Su

Robotica / Volume 33 / Issue 01 / January 2015, pp 127 - 139
DOI: 10.1017/S0263574714000125, Published online: 31 January 2014

Robotica (2015) volume 33, pp. 127–139. © Cambridge University Press 2014
doi:10.1017/S0263574714000125

Joint role exploration in sagittal balance by optimizing feedback gains

Dengpeng Xing†* and Jianbo Su‡

†*Institute of Automation, Chinese Academy of Sciences, Beijing, China*
‡*Department of Automation, Shanghai Jiao Tong University, Shanghai, China*

(Accepted December 27, 2013. First published online: January 31, 2014)

SUMMARY
This paper investigates the contributions of each joint in perturbed balance by employing multiple balance strategies and exploring gain scheduling. Hybrid controllers are developed for sagittal standing in response to constant pushes, and a hypothesis is then investigated that postural feedback gains in standing balance should change with perturbation size via an optimization approach. Related research indicates the roles of each joint: the ankles apply torque to the ground, the hips and/or arms generate horizontal ground forces, and the knees and hips squat. To investigate it from an optimization point of view, this paper uses a horizontal push of a given size, direction, and location as a perturbation, and optimizes controllers for different push sizes, directions, and locations. It applies to the ankle, hip, squat, and arm swinging strategies in standing balance. By comparing the capability of handling disturbances and investigating the feedback gains of each strategy, this paper quantitatively analyzes the contributions of each joint to perturbed balance. We believe this work is also instructive to study the progressive behavioral changes as the model gets more and more complex.

KEYWORDS: Joint roles; Perturbed balance; Optimization; Balance strategy.

1. Introduction

Humans usually use four strategies to compensate for perturbations[1]: an ankle strategy, behaving like an inverted pendulum for small perturbations; a hip strategy, employing ankle and hip actuators when the disturbance increases; a squat strategy, to flex knees and hips to lower the center of mass (CoM)[2, 3] and a step strategy if the above strategies are not sufficient to keep balance.[4] These multiple strategies reflect the biomechanical constraints faced by humans.

Horak and Nashner[4] study postural actions adopted by standing subjects adapted to changed support-surface. They demonstrate that the strategies employed are influenced by the current support conditions and the subject's experiences. Park *et al.*[5] investigate postural responses in response to perturbations of support transition by using a control system with feedback gains. The results show that the feedback gains are gradually scaled with perturbation size and can accommodate biomechanical constraints. Kuo[6] explains human selection of control strategies in response to small perturbations to stable upright balance. He linearizes the dynamic model and uses Linear Quadratic Regulators (LQR) for optimization. Alexandrov *et al.*[7] investigate equilibrium maintenance by using eigenvectors of the motion equation of a three-link sagittal model. In Kim *et al.*,[8] a feedback control model is developed to reproduce the postural responses and investigates that the postural impairments of subjects with Parkinson's disease can be described as an abnormal scaling of postural feedback gain. Kim *et al.*[9] use empirical data to fit the feedback gains in response to impulsive forces and employ the hip strategy to testify that the selection of postural gain and its scaling is dependent on type of perturbation. Compared with the robotic systems, the human movement control system has two important limitations: the gain constraints in the feedback loops of human controllers,[10] and the feedback time delays related to the various sensory motor imperfections, which can result in the instability of the movement.[7]

* Corresponding author. E-mail: xingdengpeng@hotmail.com

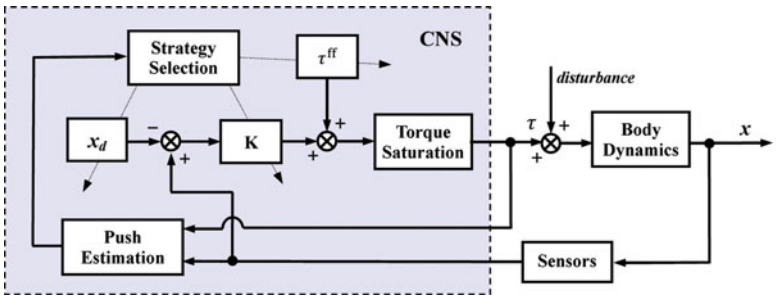

Fig. 1. (Colour online) Schematics of balance control.

To imitate those behaviors, Atkeson and Stephens[11] explore multiple strategies using the same optimization criterion for standing balance. They conclude that humanoid robots with back-drivable joints are likely to exhibit the same behavioral strategies as seen in humans. Liu and Atkeson[12] employ Differential Dynamic Programming (DDP) to generate a trajectory library of optimized control policy with adaptive grid of initial conditions. Stephens and Atkeson[13] use a linear model to approximate dynamic motion and get ground reaction forces, and employ a simplified model to predict torques and forces that are used as feedforward controls. In computer graphics, SIMBICON is developed as a simple control strategy to generate gaits and styles, and tested with pushes.[14] Yin *et al.*[15]use a data-driven approach to respond to pushes and produce interactive balancing behaviors. Our previous work addresses feedback gain optimization in response to both instantaneous and constant pushes,[16] and focuses on behavior revelation of the four balancing strategies in the sagittal plane.[17] No work has yet been presented to study gain scheduling of each strategy or give an insight into joint roles in balance with quantitative analysis. But these explain why humans employ different strategies in facing with different perturbations.

This paper explores joint roles under perturbations by investigating feedback gains and comparing performance of each balance strategy. We use pushes which may act for a period as the form of perturbation, model central nervous system (CNS) as hybrid controllers to reject disturbances and optimize feedback gains of each strategy. This paper also tests whether postural gains are scheduled with perturbation, accommodating biomechanical constraints.

2. Balance Controller Optimization

2.1. Balance controller

For an n-DoF model in the sagittal plane, the state is defined as joint angles and angular velocities, and the robot dynamics model is

$$\dot{\mathbf{x}} = \boldsymbol{f}(\mathbf{x}, \tau, F, r), \tag{1}$$

where $\mathbf{x} \in \mathbb{R}^{n\times 1}$ is the state vector, $\tau \in \mathbb{R}^{n\times 1}$ represents the joint torque, and F and r are the push size and location respectively. We assume no slipping or other change of contact state during perturbation.

Since the squat and arm swinging strategies include knees, which cannot bend forward, we consider hybrid controllers with feedback and feedforward terms. The feedback part acts on the error in each state variable, and the feedforward is determined by the push. The controller takes the form of

$$\tau = -\mathbf{K}\Delta\mathbf{x} + \tau^{ff}, \tag{2}$$

where $\mathbf{K} \in \mathbb{R}^{n\times 2n}$ is the parameter matrix, $\Delta\mathbf{x}$ represents the error between actual state and the desired state for the current push (the way to compute desired state for each push is presented in Appendix A), and τ^{ff} is the feedforward torque that only appears in the models incorporating knees reacting to negative pushes. The value of τ^{ff} is acquired by minimizing the squared sum of joint torques (See Appendix B); for positive pushes it is set as zero, i.e. $\tau_i^{ff} = 0$, and Eq. (2) is then a full state feedback controller. Figure 1 shows how the controller chooses balance strategy in response to external disturbances.

2.2. Optimization criterion

We use the same optimization criterion form as presented by Atkeson and Stephens,[11] which is defined as a weighted sum squared on the derivations of state error andthe joint torque, and probably penalty for cases violating biomechanical constraints,

$$\mathrm{L} = \begin{cases} \Delta\mathbf{x}^{\mathrm{T}}\mathbf{R}\Delta\mathbf{x} + \Delta\tau^{\mathrm{T}}\mathbf{Q}\Delta\tau & \mathbf{x}_{lim}^{-} \le \mathbf{x} \le \mathbf{x}_{lim}^{+} \\ \Delta\mathbf{x}^{\mathrm{T}}\mathbf{R}\Delta\mathbf{x} + \Delta\tau^{\mathrm{T}}\mathbf{Q}\Delta\tau + \Delta\mathbf{x}_{lim}^{\mathrm{T}}\mathbf{W}\Delta\mathbf{x}_{lim} & \text{otherwise,} \end{cases} \tag{3}$$

where $\mathbf{R} \in \mathbb{R}^{2n\times 2n}$, $\mathbf{Q} \in \mathbb{R}^{n\times n}$, and $\mathbf{W} \in \mathbb{R}^{2n\times 2n}$ are the weight matrices, $\Delta\tau = \tau - \tau^{\mathrm{ff}}$ represents the output error from the expected, or in other words, the feedback terms of each joint, and $\Delta\mathbf{x}_{lim}$ is the deviation from biomechanical constraints, which is defined as

$$\Delta\mathbf{x}_{lim} = \begin{cases} \mathbf{x} - \mathbf{x}_{lim}^{-} & \mathbf{x} < \mathbf{x}_{lim}^{-} \\ \mathbf{x} - \mathbf{x}_{lim}^{+} & \mathbf{x} > \mathbf{x}_{lim}^{+} \end{cases}.$$

The total cost function is the sum of the one step criterion over a horizon.

2.3. Optimization approach

The feedback gains are optimized for constant pushes with a number of sizes and locations. All pushes are assumed horizontal, as vertical pushes have little effect. For a constant push, based on each push size and location, we first calculate an equilibrium state, which is the posture where the subject leans into the push and the joint torque is zero or minimum (Appendix A addresses more details about how to calculate the desired state). We use this equilibrium state as the desired state, rather than the posture of standing straight up. Instead of optimizing from one initial state of standing vertically, we choose a set of initial states that evenly separate the range between the state of standing vertically and the equilibrium state to obtain robust feedback gains and converge the optimization.

SNOPT[18] is a general purpose system for constrained optimization, using sequential quadratic programming (SQP). We employ it to optimize postural gains for each push, using the LQR parameters for standing upright as initial values and optimizing the next push size with the optimal gains of the previous case. For a constant push, with the given size and location, we choose five initial states for each joint, including the posture where the subject stands straight. The cost of the trajectory from each initial state is combined and optimized gains can be generated for a wide range of pushes.

3. Multiple Strategy Implementation

3.1. The ankle strategy

With small external pushes, humans usually take the ankle strategy for balance, fixing other joints and actuating the ankles. This paper uses an inverted pendulum model, as shown in Fig. 2, with an actuator at the ankle joint to study this strategy. The model is facing to the right, and the parameters are shown in Tab. I, where the CoM is measured relative to the lower joint, and moment of inertia is about the CoM of the corresponding body. In Fig. 2, m_1 is the overall mass, including legs and upper body, l_1 is the length when standing straight, and l_{1cm} is the CoM position relative to the ankle. The biomechanical constraint includes $\theta_a \in [-0.52, 0.79]$ rad, with $\theta_a = 0$ standing for the upright state, and $\dot{\theta}_a \in [-4.6, 4.6]$ rad/s. The ankle torque is limited by the size of the foot, and here is bounded by ± 50 Nm to prevent the foot from tilting. Model parameters in this paper are taken from a preliminary design of a planned humanoid.

For the ankle strategy, the state vector is defined as $\mathbf{x} = (\theta_a, \dot{\theta}_a)^{\mathrm{T}}$, and the balance controller in Eq. (2) yields

$$\tau_a = -\begin{bmatrix} k_1 & k_2 \end{bmatrix} \begin{bmatrix} \Delta\theta_a \\ \Delta\dot{\theta}_a \end{bmatrix}. \tag{4}$$

Table I. The model parameters..

Link	Length(m)	CoM(m)	Mass(kg)	MoI(kg·m^2)
Calf	0.3304	0.1854	5.780	0.0384
Thigh	0.3306	0.2025	13.694	0.1673
Torso	0.653	0.1766	20.954	0.4599
Arm	0.67	0.3354	8.538	0.4802

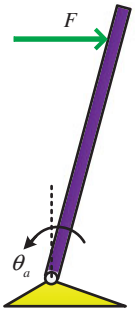

Fig. 2. (Colour online) The ankle strategy model.

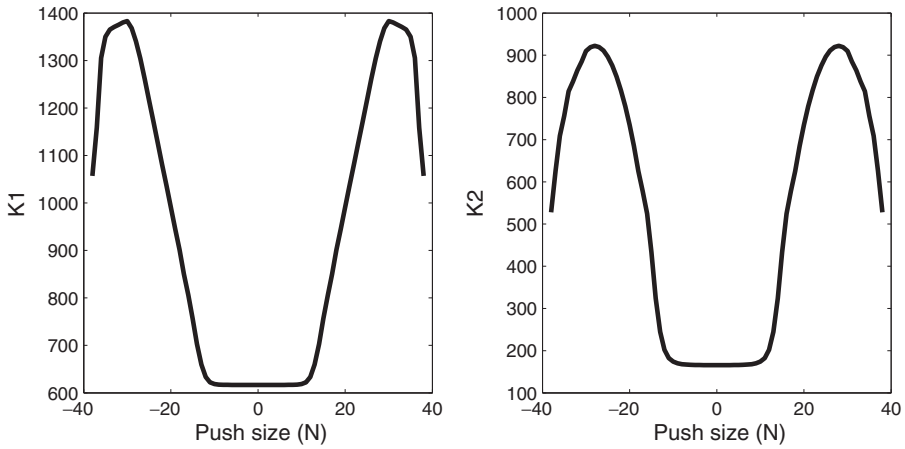

Fig. 3. The optimized gains of the ankle strategy in response to constant pushes at the head.

The one step optimization criterion without violating the constraints is expanded as

$$\mathrm{L_a} = \left(\Delta\theta_\mathrm{a}^2 + \Delta\dot{\theta}_\mathrm{a}^2\right) + 0.02\tau_\mathrm{a}^2, \tag{5}$$

where 0.02 weights the torque penalty relative to the state error in order to set the response time. During the whole responding period, state error is much smaller compared with torque. Our previous works[17] demonstrate that, in the ankle strategy, the largest state error magnitudes are less than 0.2 rad, while the torques saturate, which means the torque could reach its limit (50 Nm). In order to quickly converge to the desired states with relatively less energy consumption, the torque weight is to be appropriately small. In Atkeson and Stephens,[11] to reject impulsive perturbations, they use 0.002 as the torque and the state error weight ratio. Considering different robot models and different push types, this paper uses 0.02 as the torque weight relative to the state error. The same reason is applied for selecting weight matrix in the following strategies. To restrict trajectory behavior, we set matrix **W** of large value to avoid violating the state constraints.

Figure 3 shows the optimized gains of the ankle strategy for constant pushes at the head. The gains are symmetric when the subject is pushed forward and backward. For the pushes less than 10 N, the position feedback gain K1 ($\Delta\theta_a \rightarrow \tau_a$) and velocity feedback gain K2 ($\Delta\dot{\theta}_a \rightarrow \tau_a$) present little change with the values of 620 Nm/rad and 180 Nm·s/rad. With larger pushes ($F \in [10, 30]$ N),

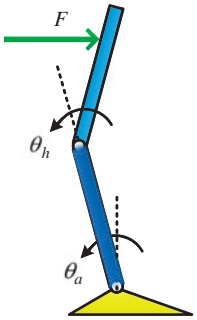

Fig. 4. (Colour online) The hip strategy model.

the gains quickly increase with the perturbation size to the maximum values of 1380 Nm/rad and 910 Nm·s/rad respectively. As the push magnitude becomes even larger, i.e. bigger than 30 N, the gains begin to exhibit fast descent. For all cases, both the gains are positive, which helps to initially lean into the push. The figures also show that the position feedback plays a more significant role for small perturbations, and the velocity feedback grows more active as the push size increases.

3.2. The hip strategy

For larger pushes, the simple ankle strategy is not suitable for balance and humans get support from the hip joint, taking advantage of large hip flexing. A two-segmented inverted pendulum model (Fig. 4) is used to simulate this strategy. The upper body is the torso and the lower body is the leg, with parameters shown in Tab. I. The hip angle is bounded by $\theta_h \in [-2.18, 0.52]$ rad, where $\theta_a = \theta_h = 0$ is the upright state. The angular velocity is limited by $\dot{\theta}_h \in [-5.5, 5.5]$ rad/s, and the hip torque is limited within ± 157 Nm.

Define the state as ankle and hip angles and angular velocities, $\mathbf{x} = (\theta_a, \theta_h, \dot{\theta}_a, \dot{\theta}_h)^{\mathrm{T}}$, and the feedback controller acts on state errors

$$\begin{bmatrix} \tau_a \\ \tau_h \end{bmatrix} = -\begin{bmatrix} k_1 & k_2 & k_3 & k_4 \\ k_5 & k_6 & k_7 & k_8 \end{bmatrix} \begin{bmatrix} \Delta\theta_a \\ \Delta\theta_h \\ \Delta\dot{\theta}_a \\ \Delta\dot{\theta}_h \end{bmatrix}. \tag{6}$$

The one step optimization function without violating the constraints expands as

$$\mathrm{L_h} = \left(\Delta\theta_{\mathrm{a}}^2 + \Delta\theta_{\mathrm{h}}^2 + \Delta\dot{\theta}_{\mathrm{a}}^2 + \Delta\dot{\theta}_{\mathrm{h}}^2\right) + 0.02\left(\tau_{\mathrm{a}}^2 + \tau_{\mathrm{h}}^2\right). \tag{7}$$

Figure 5 shows the optimized gains of the hip strategy for constant pushes at the head. The gains are symmetric except for the extreme values due to asymmetric state constraints. With a small push, i.e. less than 30 N, K1 ($\Delta\theta_a \rightarrow \tau_a$) is the largest gain with a value above 620 Nm/rad. The other three position gains are relatively small, with values no more than 100 Nm/rad. K3 ($\Delta\dot{\theta}_a \rightarrow \tau_a$) is the largest velocity gain, 170 Nm·s/rad, and the other three velocity gains have less effect, with a magnitude of less than 30 Nm·s/rad. It is also found that for small push sizes the gains gradually scale with push magnitude, with K5 ($\Delta\theta_a \rightarrow \tau_h$) and K6 ($\Delta\theta_h \rightarrow \tau_h$) gains increasing fastest and ankle torque gains related to velocities remaining almost unchanged.

With larger pushes (beyond 30 N), each gain changes much more with push magnitude, with the ankle gains increasing and the hip gains becoming more negative. The hip gains comparatively exhibit more change than the ankle gains. The most significant changes are for the gains of hip torque relative to ankle angle and velocity. For ankle gains, K3 ($\dot{\theta}_a \rightarrow \tau_a$) and K4 ($\dot{\theta}_h \rightarrow \tau_a$) change the most. Note that K5 ($\theta_a \rightarrow \tau_h$), K7 ($\dot{\theta}_a \rightarrow \tau_h$), and K8 ($\dot{\theta}_h \rightarrow \tau_h$) become negative as the push size increases, with the extreme values on the order of –370 Nm/rad, –230 Nm·s/rad, and –23Nm·s/rad respectively. The negative hip gains and the positive ankle gains take advantage of large hip flexing to initially move the ankle and the hip in the push direction, which helps in maintaining balance when the subject responds to large perturbations.

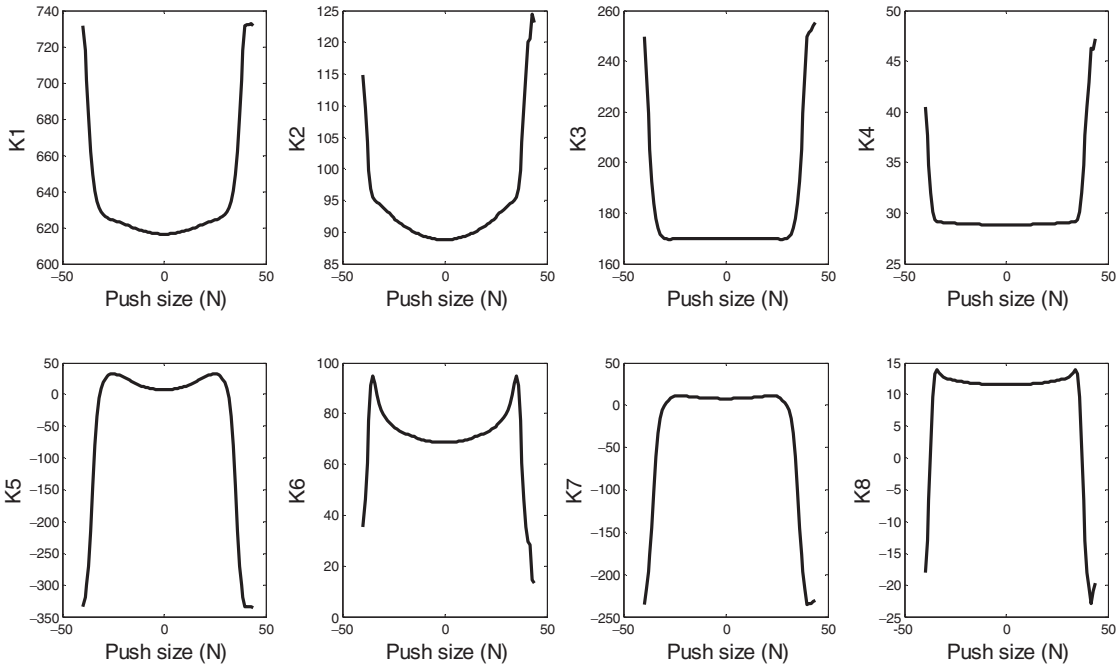

Fig. 5. The optimized gains of hip strategy in response to constant pushes at the head.

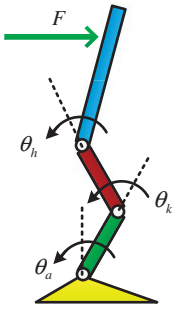

Fig. 6. (Colour online) The squat strategy model.

3.3. The squat strategy

With increasing pushes, humans employ the squat strategy to lower the CoM by flexing the hip and knee joints. The three-link model is used here to study this squat strategy, as shown in Fig. 6, where the leg is divided into the thigh and the shank, and the parameters are as shown in Tab. I. The knee angle is bounded by $\theta_k \in [-0.01, 1.87]$ rad, and the angular velocity is limited by $\dot{\theta}_k \in [-5.5, 5.5]$ rad/s. The knee torque is limited within ± 245 Nm. The knee is allowed to bend forward only a little, but a spring damper is used to model the constraint, with the spring and damping constants chosen as $K = 1000$ and $\delta = 2$.

In response to negative forces, the previous method of calculating the equilibrium state yields negative knee angles, which conflicts the property that the knee cannot bend forward. So for the squat strategy, we present different methods in computing desired states for forward and backward pushes. For a forward push, the equilibrium state is calculated as the posture that the robot leans into the push with zero joint torques. For a negative force, two types of desired states can be employed (Appendix B addresses how to compute them): the stable state at which the subject has a zero knee angle, a certain knee torque, and zero ankle and hip torques, as shown in Fig. 7(a); or the posture with a straight knee and non-zero joint torques, at which the squared sum of joint torques is minimum (Fig. 7(b); this can be achieved by using an optimization approach). Here we use the second method to generate an energy saving strategy in a long run.

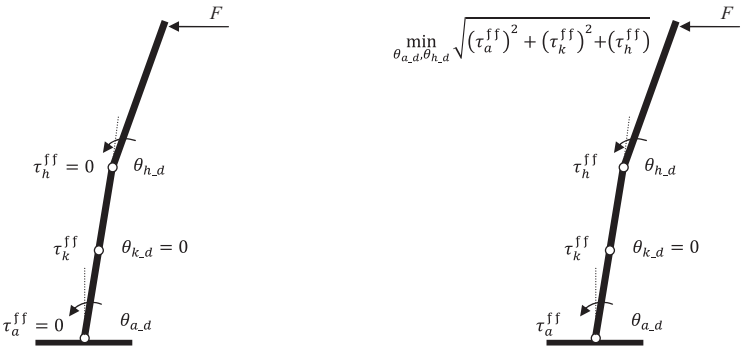

(a) Zero ankle and hip torques. (b) Minimum square sum of joint torques.

Fig. 7. Two types of desired state with a straight knee for negative pushes.

Define the state as ankle, knee, and hip angles and angular velocities, $\mathbf{x} = (\theta_a, \theta_k, \theta_h, \dot{\theta}_a, \dot{\theta}_k, \dot{\theta}_h)^{\mathrm{T}}$, and the hybrid controller leads to

$$\begin{bmatrix} \tau_a \\ \tau_k \\ \tau_h \end{bmatrix} = - \begin{bmatrix} k_1 & k_2 & \cdots & k_6 \\ k_7 & k_8 & \cdots & k_{12} \\ k_{13} & k_{14} & \cdots & k_{18} \end{bmatrix} \begin{bmatrix} \Delta\theta_a \\ \Delta\theta_k \\ \vdots \\ \Delta\dot{\theta}_h \end{bmatrix} + \begin{bmatrix} \tau_a^{\mathrm{ff}} \\ \tau_k^{\mathrm{ff}} \\ \tau_h^{\mathrm{ff}} \end{bmatrix}. \tag{8}$$

The one step optimization criterion without violating the constraints is expanded as

$$\begin{aligned} \mathrm{L} = {} & (\Delta\theta_a^2 + \Delta\theta_k^2 + \Delta\theta_h^2 + \Delta\dot{\theta}_a^2 + \Delta\dot{\theta}_k^2 + \Delta\dot{\theta}_h^2) \\ & + 0.02\left[(\tau_a - \tau_a^{\mathrm{ff}})^2 + (\tau_k - \tau_k^{\mathrm{ff}})^2 + (\tau_h - \tau_h^{\mathrm{ff}})^2\right]. \end{aligned} \tag{9}$$

The controller has 18 parameters for the squat strategy, and Fig. 8 shows a part of optimized gains (joint torque relative to its joint motion) for constant pushes at the head. The gains are asymmetric due to the non-zero feedforward torques for negative forces and the spring damper at the knees. For positive pushes, the ankle and hip gains have the same trend as the hip strategy: gradually scheduled for small pushes and significantly changed for larger forces, with the ankle gains increasing and the hip gains decreasing; and the knee gains gradually increase with push, with the extreme values of 323 Nm/rad and 132 Nm·s/rad for K8 ($\Delta\theta_k \rightarrow \tau_k$) and K11 ($\Delta\dot{\theta}_k \rightarrow \tau_k$) respectively. In response to negative pushes, all parameters start with comparatively larger values due to the feedforward torques. The knee gains increase with push, and K8 is the largest gain with the extreme value of 1548 Nm/rad; and the ankle and hip gains gradually schedule for small forces and decrease for large magnitudes of push. The significant difference for K8 between forward and backward pushes shows the effect of spring damper at the knees and the feedforward torques. With the addition of the knees, the ankles and hips possess smaller gains compared with the hip strategy. Except for different values, the gain trend is almost the same for positive and negative pushes.

3.4. The arm swinging strategy

Without taking a step, the arm swinging strategy helps humans to deal with the largest possible disturbances in the sagittal plane. It uses appropriate arm swinging with adequate squatting to reject external perturbations. We use a four-segmented model that includes ankle, knee, hip, and shoulder joints, as shown in Fig. 9, to explore this strategy. The arms are divided from the torso, with the angle bounded by $\theta_s \in [-0.5, 2.5]$ rad and the torque limited within ± 175 Nm.

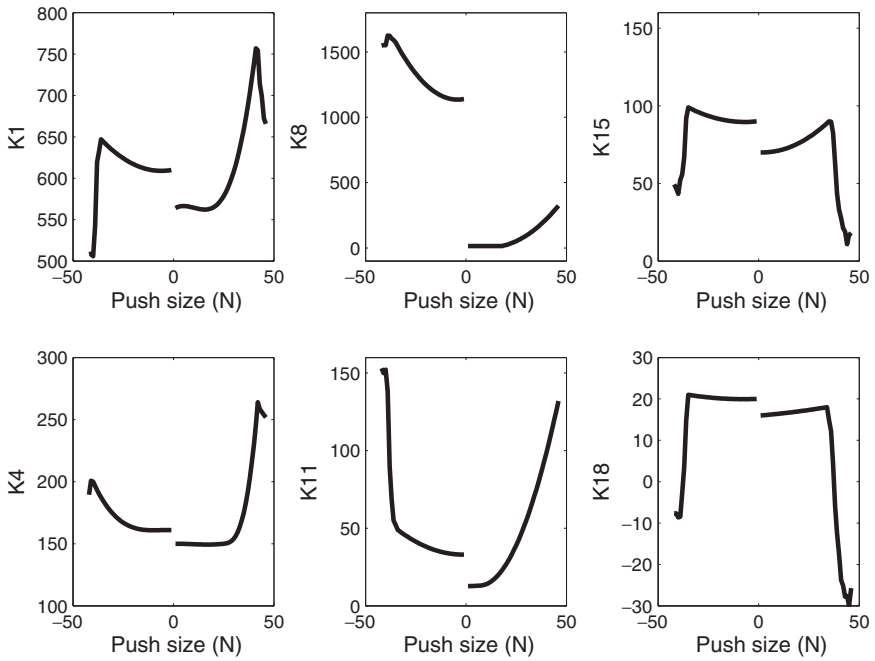

Fig. 8. Optimized gains of the squat strategy in response to constant pushes at the head.

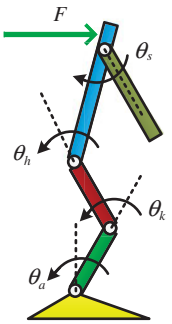

Fig. 9. (Colour online) The arm swinging strategy model.

Define the state as each angle and angular velocity, $\mathbf{x} = (\theta_a, \theta_k, \theta_h, \theta_s, \dot{\theta}_a, \dot{\theta}_k, \dot{\theta}_h, \dot{\theta}_s)^{\mathrm{T}}$. A hybrid controller yields

$$\begin{bmatrix} \tau_a \\ \tau_k \\ \tau_h \\ \tau_s \end{bmatrix} = - \begin{bmatrix} k_1 & k_2 & \cdots & k_8 \\ k_9 & k_{10} & \cdots & k_{16} \\ k_{17} & k_{18} & \cdots & k_{24} \\ k_{25} & k_{26} & \cdots & k_{32} \end{bmatrix} \begin{bmatrix} \Delta\theta_a \\ \Delta\theta_k \\ \vdots \\ \Delta\dot{\theta}_s \end{bmatrix} + \begin{bmatrix} \tau_a^{\mathrm{ff}} \\ \tau_k^{\mathrm{ff}} \\ \tau_h^{\mathrm{ff}} \\ \tau_s^{\mathrm{ff}} \end{bmatrix}. \tag{10}$$

For a backward push, the desired state is computed as the posture where the squared sum of ankle, knee, and hip torques is minimum with a straight knee and the arm is vertical with zero torque. The one step optimization cost function without violating the constraints is

$$\begin{aligned} \mathrm{L} = &(\Delta\theta_a^2 + \Delta\theta_k^2 + \Delta\theta_h^2 + \Delta\theta_s^2 + \Delta\dot{\theta}_a^2 + \Delta\dot{\theta}_k^2 + \Delta\dot{\theta}_h^2 + \Delta\dot{\theta}_s^2) \\ &+ 0.02\left[(\tau_a - \tau_a^{\mathrm{ff}})^2 + (\tau_k - \tau_k^{\mathrm{ff}})^2 + (\tau_h - \tau_h^{\mathrm{ff}})^2 + (\tau_s - \tau_s^{\mathrm{ff}})^2\right]. \end{aligned} \tag{11}$$

Controller for the arm swinging strategy has 32 parameters, and optimized joint gains relative to its joint motion are shown in Fig. 10 in response to constant pushes at the head. Since the knee cannot bend forward, the gains are also asymmetric but present approximately the same tendency as

Table II. The maximum forward pushes at the head of each strategy with upright state as the initial posture.

Push types	Ankle strategy	Hip strategy	Squat strategy	Arm swinging strategy
Impulsive	10 Ns	12 Ns	14 Ns	19 Ns
Constant	38 N	46 N	46 N	57 N

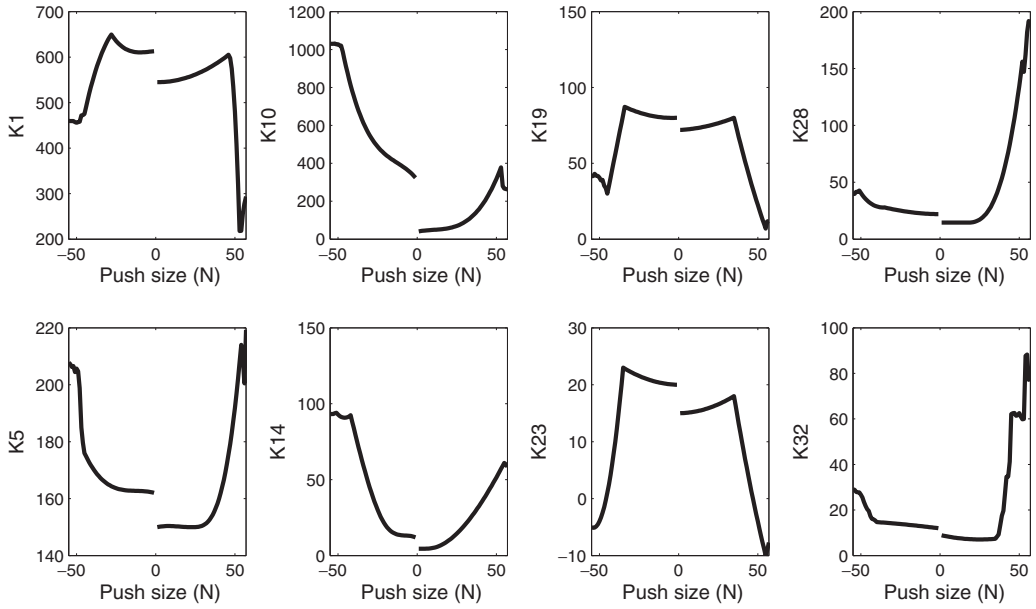

Fig. 10. The optimized gains of the arm swinging strategy in response to constant pushes at the head.

the above strategies except for different values. The ankle and hip gains gradually increase for small pushes and decrease as the push becomes larger; and the knee gains also grow larger as the push increases. The shoulder gains are little for small push sizes, but increase greatly for large positive pushes. With the addition of arms, the other joint gains show smaller magnitudes, especially that the extreme value for K10 ($\Delta\theta_k \rightarrow \tau_k$) decreases to 1030 Nm/rad. The arm swinging strategy can extend the push handling in the sagittal plane to [–55 N, 57 N].

4. Discussion

To explore the significance of each joint, the same parameters, controllers, and optimization approach have been applied to handle impulsive pushes. Standing upright is then chosen as the desired state since the instantaneous push will disappear soon. For a location, five different push sizes are employed as perturbations during optimization, including the given push magnitude, to increase the controller's robustness. Table II shows the maximum impulsive and constant pushes to the right that each strategy can handle with upright state as the initial posture. Since controllers for backward pushes in the squat and arm swinging strategies include feedforward terms, this paper only compares the forward push handling of each strategy. The ankle strategy can handle up to 38 N constant push and 10 Ns impulse, but falls down for bigger pushes. Adding the hip joints, the hip strategy can extend the maximum push handling to 12 Ns impulse and 46 N constant push by taking advantage of large hip flexing. With contributions of the knee joints, the squat strategy has little effect on the constant push response but expands the impulse handling to 14 Ns, showing the influence of lowering CoM. Because of appropriate arm swinging compensation, the arm swinging strategy can handle up to 19 Ns impulse and 57 N constant push.

Since controllers of different strategies have different number of gains, a part of parameter comparison is shown in Fig. 11, where gains of joint torque relative to its joint motion are presented. The ankle strategy relies entirely on the ankles and has much large ankle gains. With the addition of hip joints, the hip strategy presents much smaller ankle gains for large pushes: the maximum

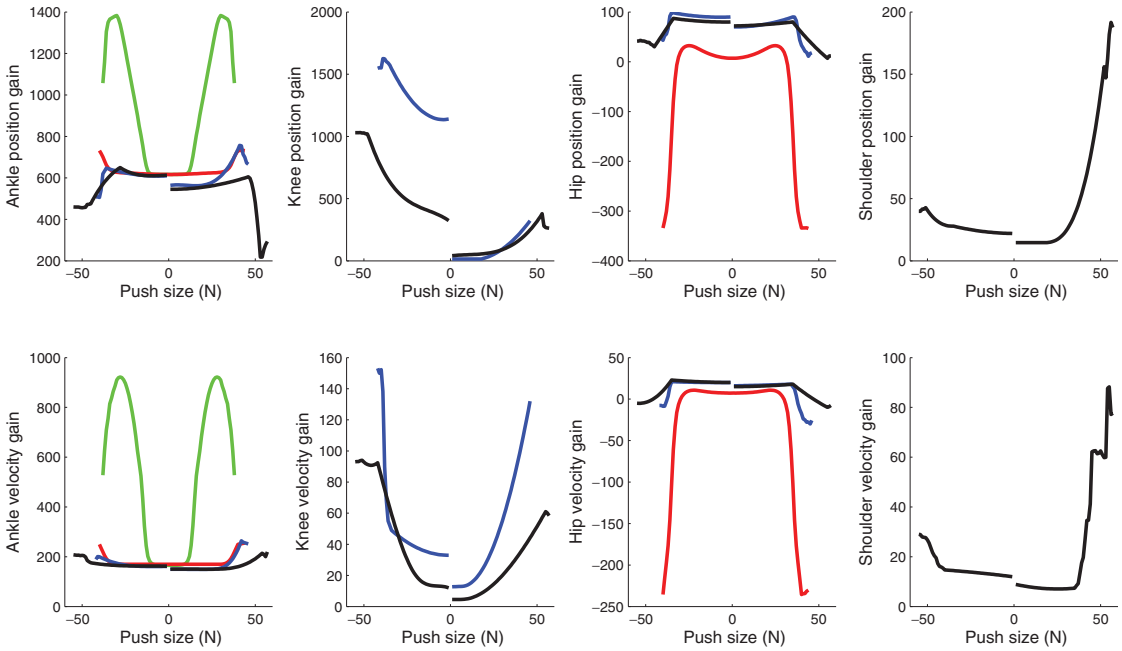

Fig. 11. (Colour online) Feedback gain comparison between different strategies. Green, red, blue, and black lines represent the ankle, hip, squat, and arm swinging strategies respectively.

ankle position gain ($\Delta\theta_a \rightarrow \tau_a$) drops from almost 1400 Nm/rad to less than 740 Nm/rad, and the ankle velocity gain ($\Delta\dot{\theta}_a \rightarrow \tau_a$) decreases from 900 Nm·s/rad to less than 260 Nm·s/rad. The squat strategy has the same gain scheduling trend at the ankle and hip joints compared with the hip strategy, with much less values, especially for the hip gains, owing to the contributions from knee squatting. For small pushes, the squat strategy has relatively bigger hip gains and smaller ankle gains; and for big pushes, the ankle gains are not quite different but the hip gains become much smaller. The extreme hip position gain ($\Delta\theta_h \rightarrow \tau_h$) changes from –370 Nm/rad to 18 Nm/rad, and the hip velocity gain ($\Delta\dot{\theta}_h \rightarrow \tau_h$) changes from –230 Nm·s/rad to –30 Nm·s/rad. With proper arm compensation, the arm swinging strategy presents significant knee gain changes while maintaining the same trend of other gains as the squat strategy, with relative lower magnitudes. The maximum knee position gain ($\Delta\dot{\theta}_k \rightarrow \tau_k$) for backward push reduces from 1630 Nm/rad to 1030 Nm/rad, and the knee velocity gain ($\Delta\dot{\theta}_k \rightarrow \tau_k$) reduces from 153 Nm·s/rad to 93 Nm·s/rad (negative push) and from 132 Nm·s/rad to 61 Nm·s/rad (forward push). The shoulder gains are small: the maximum values are 190 Nm/rad for the position gain ($\Delta\dot{\theta}_s \rightarrow \tau_s$) and 85 Nm·s/rad for the velocity gain ($\Delta\dot{\theta}_s \rightarrow \tau_s$). In summary, compared with the previous strategy, the additional joint greatly decreases the other joint gains: the hip strategy has much lower ankle gains; the squat strategy gives smaller hip gains; and the arm swinging strategy reduces about 1/3 of the knee gains (backward push). Known from the gain comparison, in all strategies the ankle gains are the largest for small pushes, which demonstrates that the ankles play a foremost role in balancing small perturbations. As the push increases, other joints gradually become more active and share ankles' burden.

Table II, Figure 11, and the above analysis show that each joint contributes in handling external disturbances. The ankles interact with the environment and supply torques to keep balance. They also determine the CoM horizontal position. The hip joints change the trajectory of the CoM by varying the relative posture between upper and lower bodies, and the large forward hip flexing improves the handling capability of the hip strategy. The knees lower the CoM and their big backward bending expands the handling of instantaneous disturbances. The addition of shoulder joints separates the arms from the torso and balances bigger perturbations by adequately swinging the arms to generate appropriate reverse moments. For bigger pushes which the arm swinging strategy cannot handle, a step has to be taken. It coincides with the observation of human responses to disturbances: the ankles apply torque to the ground; the hips and arms generate horizonal ground forces; and the knees and hips squat.[11]

It is worth to be noted that in human movement research, Alexandrov *et al.*[10,19,20] study the hip strategy with subjects standing on a movable platform and use the control of the motion equation eigenvectors instead of the control of separate joint angles as proposed by this paper. The movement control is then simplified by using eigenvector control variables, since the feedback gain matrices K in each strategy become diagonal. This method can effectively deal with the gain constraints in human controllers such as muscle strength. It is also demonstrated that, to select optimal feedback gains (joint stiffness and viscosity) that provide movement stability and the fastest responses to perturbations, the relatively large time delays in human perturbation responses can be overcome.[7] In robotic systems, we also need to select appropriate feedback gains to acquire stability and fast response in experiments because of disturbance and time delay.

5. Conclusions

This paper explores gain scheduling in standing balance and investigates the roles of each joint under perturbations. To achieve this, we study multiple balance strategies and optimize controllers in response to various pushes. We explore gain change with perturbation size. It appears that feedback gains gradually scale with push magnitude for small pushes and change significantly for large pushes. From the optimized feedback gains, we also find that the ankle joints play an important role for small perturbations while the hip, knee, and shoulder joints grow more active as the push increases.

We investigate the role of each joint in standing balance. As we include more joints, the robot can handle larger pushes. By comparing the maximum push handling and feedback gains of each strategy, role of joints can be typically concluded as follows: The ankles apply torque to the ground; the knees and hips squat, with knees lowering the CoM and hips changing the horizontal trajectory of the CoM; and the arms generate proper reverse moments.

Acknowledgment

This material was supported by the Program of National Nature Science Foundation of China (NSFC 61305115, and NSFC Key project no. 61221003).

References

1. C. F. Runge, C. L. Shupert, F. B. Horak and F. E. Zajac, "Ankle and hip postural strategies defined by joint torques," *Gait Posture* **10**(2), 280–289 (2001).
2. H. Hemami, K. Barin and Y. C. Pai, "Quantitative analysis of the ankle strategy under translational platform disturbance," *IEEE Trans. Neural Syst. Rehabil. Eng.* **14**(4), 470–480 (2006).
3. L. Nashner and G. McCollum, "The organization of postural movements: A formal basis and experimental synthesis," *Behav. Brain Sci.* **8**(1), 135–150 (1985).
4. F. Horak and L. Nashner, "Central programming of postural movements: Adaptation to altered support-surface configurations," *J. Neurophysiol.* **55**(6), 1369–1381 (1986).
5. S. Park, F. B. Horak and A. D. Kuo, "Postural feedback responses scale with biomechanical constraints in human standing," *Exp. Brain Res.* **154**(4), 417–427 (2004).
6. A. D. Kuo, "An optimal control model for analyzing human postural balance," *IEEE Trans. Biomed. Eng.* **42**(1), 87–101 (1995).
7. A. V. Alexandrov, A. A. Frolov, F. B. Horak, P. Carlson-kuhta and S. Park, "Feedback equilibrium control during human standing," *Biol. Cybern.* **93**(5), 309–322 (2005).
8. S. Kim, F. B. Horak, P. Carlson-Kuhta and S. Park, "Postural feedback scaling deficits in Parkinson's disease," *J. Neurophysiol.* **102**, 2910–2920 (2009).
9. S. Kim, C. G. Atkeson and S. Park, "Perturbation-dependent selection of postural feedback gain and its scaling," *J. Biomech.* **45**(8), 1379–1386 (2012).
10. A. V. Alexandrov and A. A. Frolov, "Closed-loop and open-loop control of posture and movement during human upper trunk bending," *Biol. Cybern.* **104**(6), 425–438 (2011).
11. C. G. Atkeson and B. J. Stephens, "Multiple Balance Strategies from One Optimization Criterion," *Proceedings of the International Conference on Humanoid Robots* (2007) pp. 57–64.
12. C. Liu and C. G. Atkeson, "Standing Balance Control Using a Trajectory Library," *Proceedings of the International Conference on Intelligent Robots and Systems* (2009) pp. 3031–3036.
13. B. Stephens and C. G. Atkeson, "Modeling and Control of Periodic Humanoid Balance Using the Linear Biped Model," *Proceedings of the International Conference on Humanoid Robots* (2009) pp. 379–384.
14. K. Yin, K. Loken and M. van de Panne, "SIMBICON: Simple biped locomotion control," *ACM Trans. Graph.* **26**(3), 150:1–10 (2007).

15. K. Yin, D. K. Pai and M. Van de Panne, "Data-driven interactive balancing behaviors," *Proceedings of the Pacific Graphics* (2005) pp. 118–121.
16. D. Xing, C. G. Atkeson, J. Su and B. J. Stephens, "Gain Scheduled Control of Perturbed Standing Balance," *Proceedings of the IEEE International Conference on Intelligent Robots and Systems* (2010) pp. 4063–4068.
17. D. Xing and X. Liu, "Multiple balance strategies for humanoid standing control," *Acta Autom. Sin.* **37**(2), 234–239 (2011).
18. P. E. Gill, W. Murray and M. A. Saunders, "SNOPT: An SQP algorithm for large-scale constrained optimization," *SIAM J. Optim.* **12**(4), 979–1006 (2002).
19. A. V. Alexandrov, A. A. Frolov and J. Massion, "Biomechanical analysis of movement strategies in human forward trunk bending. I. Modeling," *Biol. Cybern.* **84**, 425–434 (2001).
20. A. V. Alexandrov, A. A. Frolov and J. Massion, "Biomechanical analysis of movement strategies in human forward trunk bending. II. Experimental study," *Biol. Cybern.* **84**, 435–443 (2001).

Appendix A. Desired state calculation for models without considering straight knees

For an n-DoF model without knees, as shown in Fig. 12, the desired state is an equilibrium state, which is the posture where the subject leans into the push and the torque at each joint is zero. The overall moment of link n about joint n is zero at the equilibrium state, which leads to

$$\sum_{i=1}^{n} \theta_{i\_d} = \arctan \frac{Fr'}{m_n g l_{n\_cm}}, \tag{12}$$

where r' is the push position relative to joint n, $\sum_{i=1}^{n} \theta_{i\_d}$ is the sum of all joint angles and is also the angle between link n and the vertical line. Consider links n and $n-1$, we have the following moment equilibrium equation about joint $n-1$,

$$\begin{aligned}(m_n g l_{n-1} + m_{n-1} g l_{n-1\_cm}) \sin\left(\sum_{i=1}^{n-1} \theta_{i\_d}\right) - F l_{n-1} \cos\left(\sum_{i=1}^{n-1} \theta_{i\_d}\right) \\ = Fr' \cos\left(\sum_{i=1}^{n} \theta_{i\_d}\right) - m_n g l_{n-1} \sin\left(\sum_{i=1}^{n} \theta_{i\_d}\right).\end{aligned} \tag{13}$$

By substituting Eq. (12) into Eq. (13) and using $\theta_{n\_d} = \sum_{i=1}^{n} \theta_{i\_d} - \sum_{i=1}^{n-1} \theta_{i\_d}$, we can get the desired posture for link n. The other desired states can be computed iteratively.

Appendix B. Desired state calculation for negative pushes with models incorporating knees

When the model includes knees and corresponds to negative pushes, the desired state is calculated in different ways. Since the knees cannot bend forward, there are typically two methods to compute the desired state for a given backward push. One method is to compute the state at which the subject leans forward and has a zero knee angle and a certain knee torque, and zero torques at other joints.

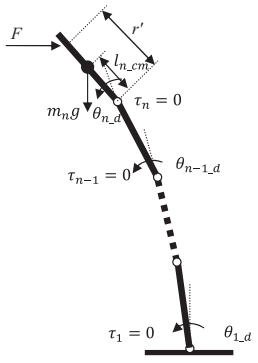

Fig. 12. The desired state calculation diagram.

Suppose k joint is the knees. By following the above iterative method, we could get values from $\sum_{i=1}^{n} \theta_{i\_d}$ to $\sum_{i=1}^{k+1} \theta_{i\_d}$, and then we have the moment equilibrium equation at the knees:

$$F\left[r' \cos\left(\sum_{i=1}^{n} \theta_{i\_d}\right) + \sum_{j=k}^{n-1} l_j \cos\left(\sum_{i=1}^{j} \theta_{i\_d}\right)\right] = \sum_{j=k}^{n} m_j g l_{j\_cm} \sin\left(\sum_{i=1}^{j} \theta_{i\_d}\right) + \sum_{ii=k+1}^{n} m_{ii} g \left[\sum_{j=k}^{ii-1} l_j \sin\left(\sum_{i=1}^{j} \theta_{i\_d}\right)\right] + \tau'_k, \tag{14}$$

where $\theta_{k\_d} = 0$ represents the straight knees and τ'_k is the knee torque at this equilibrium state. The result of Eq. (14) is the feedforward term at the knees and the corresponding posture can be set as the desired state. The other desired states from joint $k-1$ to joint 1 can be computed using the previous iterative method with the knee torque τ'_k.

This paper uses another method, which is to calculate the posture with a straight knee and non-zero joint torques. In order to generate an energy saving policy for a long time, this posture should have a minimum squared sum of joint torques. The moment equilibrium equation about joint m yields

$$\tau'_m = F\left[r' \cos\left(\sum_{i=1}^{n} \theta_{i\_d}\right) + \sum_{j=m}^{n-1} l_j \cos\left(\sum_{i=1}^{j} \theta_{i\_d}\right)\right] - \sum_{j=m}^{n} m_j g l_{j\_cm} \sin\left(\sum_{i=1}^{j} \theta_{i\_d}\right) - \sum_{ii=m+1}^{n} m_{ii} g \left[\sum_{j=m}^{ii-1} l_j \sin\left(\sum_{i=1}^{j} \theta_{i\_d}\right)\right]. \tag{15}$$

We use an optimization approach to determine the joint torques, which minimizes the criterion of

$$\mathrm{L}'(\theta_{1\_\mathrm{d}}, \ldots, \theta_{\mathrm{n\_d}}) = \sqrt{\sum_{\mathrm{i}=1}^{\mathrm{n}} \tau_{\mathrm{i}}'^2}. \tag{16}$$

Equation (15) and the minimization of Eq. (16) may lead to non-unique results. We choose the posture which is the closest to the upright state, and the corresponding joint torques constitute the feedforward terms as listed in Eqs. (8) and (10), i.e. τ_i^{ff}. After acquiring the joint torques, we can use the iterative algorithm to calculate the desired angle of each joint at which the moment equilibrium equation at each joint is satisfied.